Journal Pre-proof

Quantitative Evaluation of (0001) Sapphire Recession in High-Temperature High-Velocity Steamjet Exposures

Mackenzie J. Ridley, Elizabeth J. Opila

PII: S0955-2219(21)00552-5

DOI: https://doi.org/10.1016/j.jeurceramsoc.2021.07.064

Reference: JECS 14240

To appear in: *Journal of the European Ceramic Society*

Received Date: 5 July 2021

Accepted Date: 28 July 2021

Please cite this article as: Ridley MJ, Opila EJ, Quantitative Evaluation of (0001) Sapphire Recession in High-Temperature High-Velocity Steamjet Exposures, *Journal of the European Ceramic Society* (2021), doi: https://doi.org/10.1016/j.jeurceramsoc.2021.07.064

Quantitative Evaluation of (0001) Sapphire Recession in High-Temperature High-Velocity Steamjet Exposures

Mackenzie J. Ridley, Elizabeth J. Opila

University of Virginia, Materials Science and Engineering

8/4/2021

Abstract: High-temperature high-velocity steam exposures of (0001) sapphire coupons were performed at temperatures of 1200 °C-1450 °C to determine the quantitative capability of the steamjet apparatus. Recession results were compared to calculated values of $Al(OH)_3$ (g) mass transfer rates based on laminar flow models and available thermodynamic data for $Al(OH)_3$ (g). Linear material volatilization rates and a strong gas velocity dependence on the reaction depth confirmed that the Al_2O_3 reaction was controlled by a gas-phase diffusion process. The temperature dependence for the steam reaction agreed with thermodynamic calculations and with the literature, confirming that $Al(OH)_3$ (g) transport through a gas boundary layer represents the rate-limiting step for Al_2O_3 volatilization in steam. The steamjet experimental setup can thus be utilized for determination of steam-oxide reaction thermodynamics given known steam flow conditions. Steamjet test recession results for simple oxides are discussed for comparison with behavior of complex oxides that form porous product layers, which are not yet well understood.

1. Introduction

High-temperature stabilities of metal oxides in steam environments represent an active are of research in materials design for power generation and propulsion applications. Heat exchangers and solid oxide fuel cell (SOFC) utilize Cr-rich alloys, where the resulting Cr_2O_3-rich thermally grown oxide can react with steam to form a volatile chromium oxyhydroxide gas species [1], [2]. Ceramic electrolytes and amorphous sealing glasses in SOFCs can contain

species that react with steam to also decrease effective component lifetimes and hermeticity between stacks [3], [4]. Predicting oxide-steam reactions is a primary interest for environmental barrier coatings (EBCs). EBCs are required coatings for application of SiC ceramic matrix composites (CMCs) in turbine engine hot sections. A principle requirement of the EBC layer is to protect the CMC from high-temperature high-velocity reactions with steam, a known byproduct of fuel combustion. Current generation EBCs are known to also react with steam to produce volatile gas species, although EBC reactivities are greatly reduced compared to that of SiC due to a decreased silica activity. A generalized steam reaction for a metal oxide (MO) silicate compound is presented in Equation 1, where production of a volatile hydroxide species and a porous, silica-depleted reaction product are expected.

$$MO\cdot(SiO_2)_n + 2\ H_2O(g) = Si(OH)_4(g) + MO\cdot(SiO_2)_{n-1} + \text{porosity} \quad (1)$$

Thermogravimetric analysis (TGA) and low velocity steam testing are most commonly reported in the literature, although low steam partial pressures and low gas velocities can result in different steam reaction mechanism and can introduce impurity contamination to lab tested samples [5]–[8]. The inlet gas velocity for a Model 501-K turbine (Rolls-Royce, Indianapolis, IN) field test at vane mid-span was measured at ~160 m/s, and the gas stream was further accelerated to ~575 m/s near the vane exit [9].To best model a turbine hot section, high-temperature high-velocity steam testing of EBCs is required for understanding coating lifetimes in service. The quantitative nature of one such high-velocity steam experimental setup, termed a steamjet [10], [11], has yet to be validated.

The volatilization kinetics for oxides in steam are believed to be rate-limited by hydroxide gas phase diffusion through a boundary layer [12]. Assuming laminar flow conditions and a flat plate geometry, the flux of metal hydroxide leaving the sample surface, J_l, can be

defined as Equation 2, where Re is the Reynolds number, Sc is the Schmidt number, D_{AB} is the gas interdiffusion coefficient for the metal hydroxide in the water vapor phase, ρ' is the equilibrium concentration of metal hydroxide at the sample surface, and L is the characteristic sample length [13]. The Reynolds and Schmidt numbers are expanded in Equation 2, where ρ is the concentration of water vapor in the boundary layer, v is the water vapor velocity, and μ is the gas viscosity [13].

$$J_l = 0.664(Re)^{\frac{1}{2}}(Sc)^{\frac{1}{3}}\frac{D_{AB}\rho'}{L} = 0.664\left(\frac{\rho v L}{\mu}\right)^{\frac{1}{2}}\left(\frac{\mu}{\rho D_{AB}}\right)^{\frac{1}{3}}\frac{D_{AB}\rho'}{L} \quad (2)$$

Mass transfer of the metal hydroxide phase is proportional to the oxide recession rate through the oxide density, ρ_{oxide}. Equation 2 can be simplified through controlled steamjet exposures with constant water vapor velocity, water vapor partial pressure, gas viscosity, and sample length, shown in Equation 3.

$$k_l \propto \frac{J_l}{\rho_{oxide}} \propto D_{AB}\rho' \quad (3)$$

The gas interdiffusion coefficient and metal hydroxide partial pressure both display temperature dependences, which can be determined from k_l through an experimental test matrix with varied exposure time and temperatures for the steamjet experimental setup.

The temperature dependence for a given steam reaction is useful for development of lifetime prediction models for EBC/CMC systems in service. Additionally, the temperature dependence allows for determination of the volatilized hydroxide reaction product through comparison to the oxide-steam reaction enthalpy. Experimental determination of the reaction enthalpy through the measured temperature dependences can in turn provide information on the primary reaction product species through comparison to thermodynamic data. Candidate EBC compositions have been analyzed after exposure to a high-velocity steamjet setup, where reaction enthalpies were calculated from mass loss and recession data to determine temperature

dependences for the steam reactions occurring. Equilibrium at the oxide-steam interface and laminar flow are assumed to calculate reaction enthalpies. Selective SiO_2 volatilization from complex silicate compounds $HfSiO_4$ [14] and $Yb_2Si_2O_7$ [15] in previous studies were expected to result in a reaction enthalpy similar to that of pure SiO_2, yet experimental values were much higher than predicted. In contrast, the temperature dependence for the complete volatilization of $Ba_{0.75}Sr_{0.25}Al_2Si_2O_8$ (BSAS) in high-velocity steam agreed with initial thermodynamic calculations for formation of Ba-, Sr-, Al-, and Si- hydroxide species [16]. The quantitative nature of the steamjet experimental setup had not yet been verified for simple oxides, whose thermodynamic and kinetic properties are well studied compared to complex compounds.

Table 1 displays the steam reactions for various materials, along with material melting temperatures and estimated reaction enthalpies from Meschter et al. [17]. Each material has been categorized by the dominant metal (M) hydroxide product phase, $M(OH)_x$ (g). The temperature dependences for the presented oxides range from 150 – 300 kJ/mol, with the exception of SiO_2. The presence of alumina furnace ware has prevented quantitative analysis of most oxides in the steamjet, where alumina deposition or reaction to form aluminate compounds rapidly occur. Exposure of amorphous SiO_2 in the steamjet has been attempted, yet material shearing from high gas velocities and devitrification prevented accurate baseline measurements from being determined. Additionally, crystalline SiO_2 (cristobalite) has multiple polymorph transitions and associated volume changes up to the temperature ranges of interest which result in material cracking upon entry and removal of samples from the furnace. Thus, steam exposures of high-purity single crystal Al_2O_3 represent the clearest route for analysis of the temperature dependence of simple oxide volatilization in the steamjet.

Table 1. Oxide reaction enthalpies for formation of metal hydroxide gas species upon steam reaction, from [17].

Oxide	Reaction Enthalpy, ΔH_{rxn}, kJ/mole	Steam Reaction	Oxide Melting Temperature, °C
MgO	271	$MgO + H_2O = Mg(OH)_2$ (g)	2852
CaO	266	$CaO + H_2O = Ca(OH)_2$ (g)	2572
SrO	238	$SrO + H_2O = Sr(OH)_2$ (g)	2531
BaO	163	$BaO + H_2O = Ba(OH)_2$ (g)	1923
Y_2O_3	290	$0.5\ Y_2O_3 + 1.5\ H_2O = Y(OH)_3$ (g)	2425
Al_2O_3	185	$0.5\ Al_2O_3 + 1.5\ H_2O = Al(OH)_3$ (g)	2072
ZrO_2	210	$ZrO_2 + 2\ H_2O = Zr(OH)_4$ (g)	2715
SiO_2	54	$SiO_2 + 2\ H_2O = Si(OH)_4$ (g)	1710

High-velocity steam exposures were performed on basal plane (0001) sapphire to determine the reaction kinetics for the following:

$$1/2\ Al_2O_3 + 3/2\ H_2O \rightarrow Al(OH)_3\ (g) \qquad (4)$$

Alumina furnace ware reacts with water vapor to also form the $Al(OH)_3$ (g) species, such that low velocity regions of the samples were expected to have suppressed steam reactions due to saturation of hydroxide species in the gas boundary layer. At the high velocities of interest, a water vapor partial pressure of 1 atm promoted the steam volatilization of sapphire.

Material recession depths and mass loss data were utilized to calculate the temperature dependence for $Al(OH)_3$ (g) formation from 1200 °C – 1450 °C as a comparison to data from FactSage thermodynamic database and from the literature. Calculated reaction enthalpies of oxides and complex compounds in the steamjet are discussed.

2. Methods

A modified horizontal tube furnace (Model 1730-12 HTF, CM Furnace Inc., Bloomfield,

NJ), termed a steamjet, was used in this research to achieve environments relevant for turbine engines. The steamjet simulates a 10 atm turbine engine environment containing 10% H_2O (g) by maintaining 1 atm steam [18]. The experimental design, shown in Figure 1, originated from Dos Santos et al. [18] with further modifications by Golden, Parker, and Opila [10], [11]. Deionized water is pumped into a 1 mm diameter platinum/rhodium alloy capillary passing through a 900 °C preheater and into the tube furnace hot zone. Argon flows in the tube furnace at 30 sccm around the outer surface of the platinum capillary to limit PtO_2 (g) formation from the capillary. The water in the capillary vaporizes in the preheater section and undergoes the liquid-gas volume expansion, which accelerates steam flow into the tube furnace hot zone.

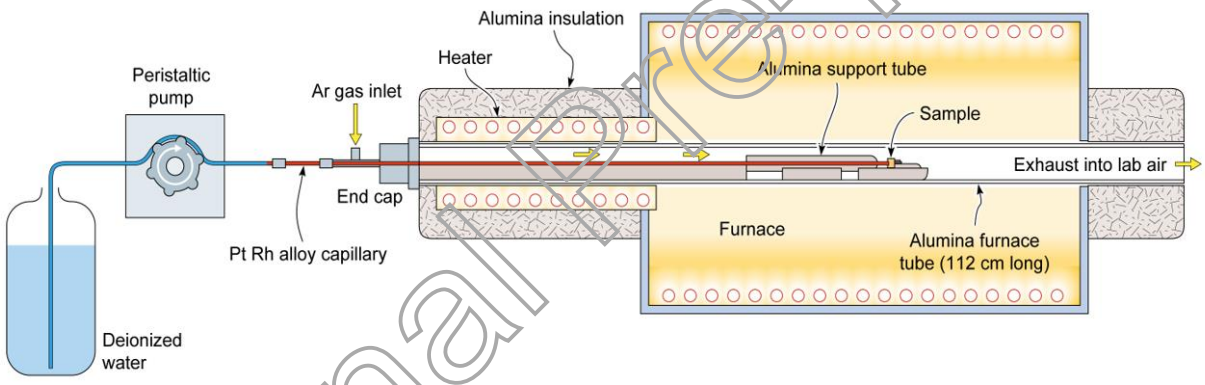

Figure 1. High velocity steamjet experimental setup [11].

The sample is held in place on an Al_2O_3 holder with platinum wire at a 45-degree angle relative to the capillary outlet, as shown in Figure 2. Platinum foil is used between the sample and Al_2O_3 holder to limit direct contact contamination. The test specimen is placed 1 mm away from the capillary exit in the furnace hot zone, where the proximity of the sample to the capillary outlet allows for high-velocity steam to impinge upon sample surface with a water vapor partial

pressure of 1 atm, thus preventing tube furnace impurities from reacting with most of the coupon face.

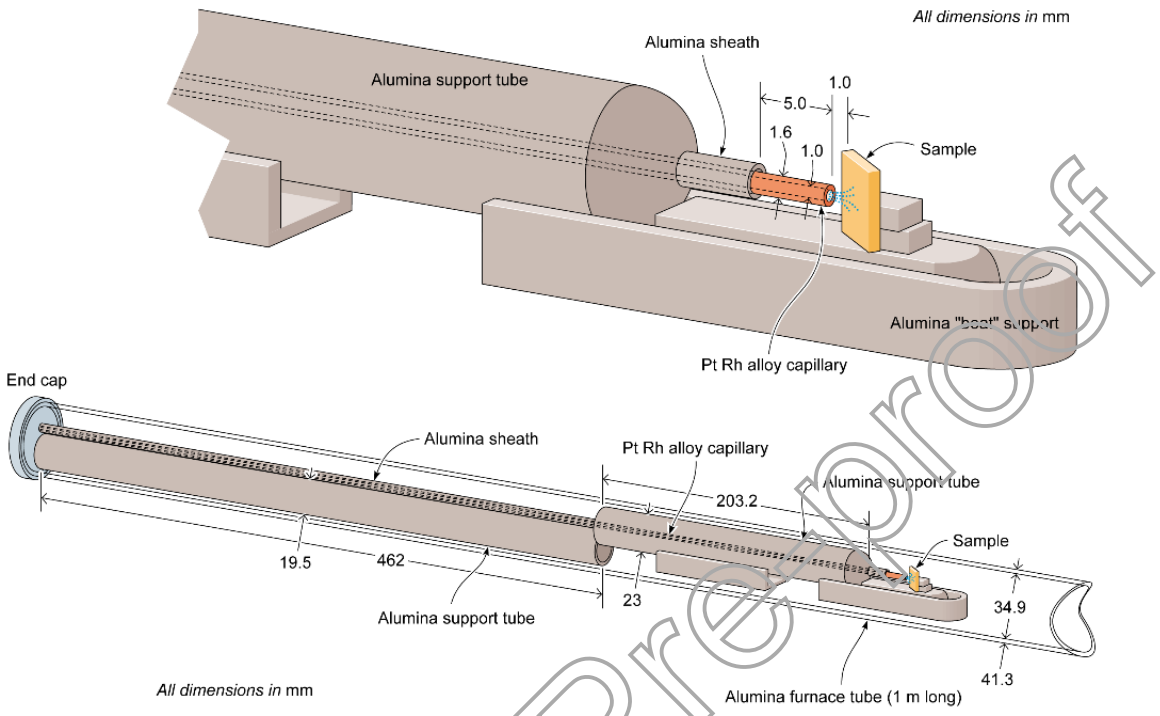

Figure 2. Sample view of high velocity steamjet experimental setup [11].

Gas velocities are experimentally controlled through input of the liquid water flow rate (1.65 ml/min) and experimental setup geometry. ANSYS (Canonsburg, PA) computational fluid dynamics software is used to model the water vapor velocity distribution across the surface of the sample. A maximum velocity of ~204 m/s at 1450 °C is calculated for a 1.65 ml/min liquid water flow rate, as shown in Figure 3. ANSYS velocity maps are used to correlate local recession depths and microstructural features to a water vapor velocity.

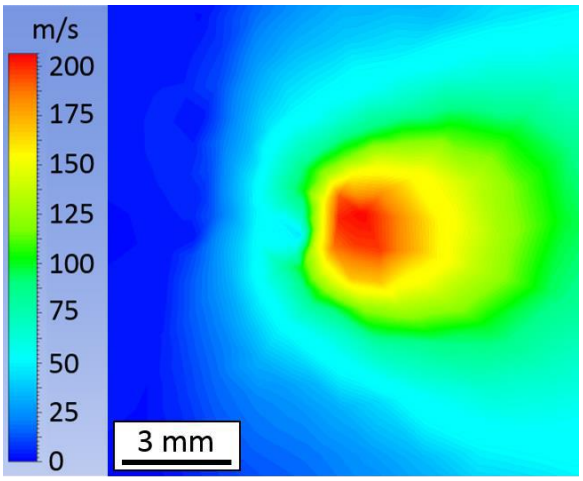

Figure 3. ANSYS Computational Fluid Dynamics Model for steam velocity distribution across the sample face at 1400 °C.

High-purity (99.996%) c-plane Al_2O_3 (0001) samples were purchased from MTI Corporation (Richmond, Ca.) as 10 x 10 x 1 mm coupons with both faces polished to less than 5 Å average roughness. In this study, c-plane Al_2O_3 samples were loaded into the furnace at ~100 °C/min with the steam already flowing to prevent sample cracking. Sample exposures were performed at 1200 °C, 1300 °C, 1400 °C, and 1450 °C for a range of exposure times from 6-84 hours. Sample mass was recorded for each specimen (MS105DU, Mettler-Toledo, Columbus, OH) before and after steam exposures. Samples were then sputter coated with a reflective gold/palladium alloy film for production of surface topography maps via white light profilometry (Zygo: NewView 7300: Middlefield, CT). Recession linescans were created with Mountain Maps software (Digital Surf, France) to determine the maximum recession depths for each sample, with the unreactive sample regions as references to the initial sample heights. The maximum sample recession corresponded to the maximum calculated steam velocity and was used for analysis of the Al_2O_3 (0001) steam reaction alongside specific mass loss data. The reported errors for the specific mass loss and maximum recession data were determined from the best fit slopes for each exposure temperature.

3. Results

The FactSage SGPS database was used to calculate the equilibrium partial pressure of $Al(OH)_3$ (g) for the reaction in Equation 4 from 1000 °C – 1500 °C, as shown in Figure 4. $Al(OH)_3$ (g) is the dominant hydroxide species expected to form. The next most stable aluminum hydroxide species was $Al(OH)_2$ (g) with a partial pressure of $1.1x10^{-10}$ atm at 1500 °C. Formation of all $Al(OH)_x$ (g) species besides $Al(OH)_3$ (g) were considered negligible and were not accounted for in the conducted analysis.

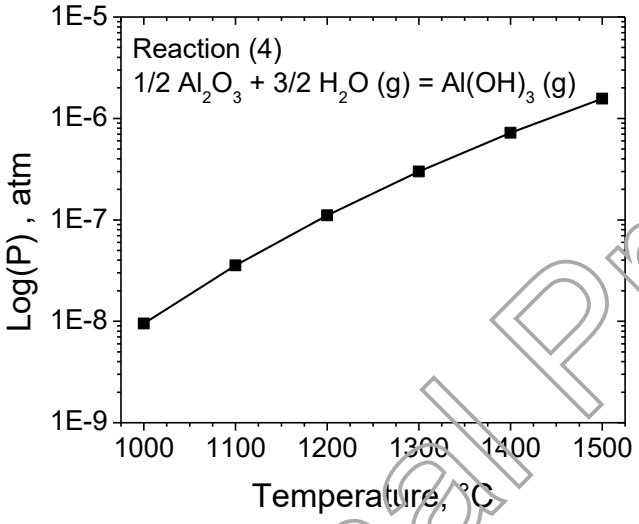

Figure 4. $Al(OH)_3$ (g) partial pressures from reaction (4), calculated with FactSage SGPS database for 1 atm H_2O (g).

Profilometer maps for three Al_2O_3 (0001) samples after steam exposure for 24 hours are presented in Figure 5, where each profile has the same color scale corresponding to the surface depth. The 1 mm circular impingement site on each sample increases in relative depth with increasing temperature, corresponding to increased Al_2O_3 volatilization at the highest steam velocities. The left side of each sample is upstream of the gas flow direction. Negligible steam reactivity occurred in the upstream regions, which provided references for the maximum recession depth at the impingement site.

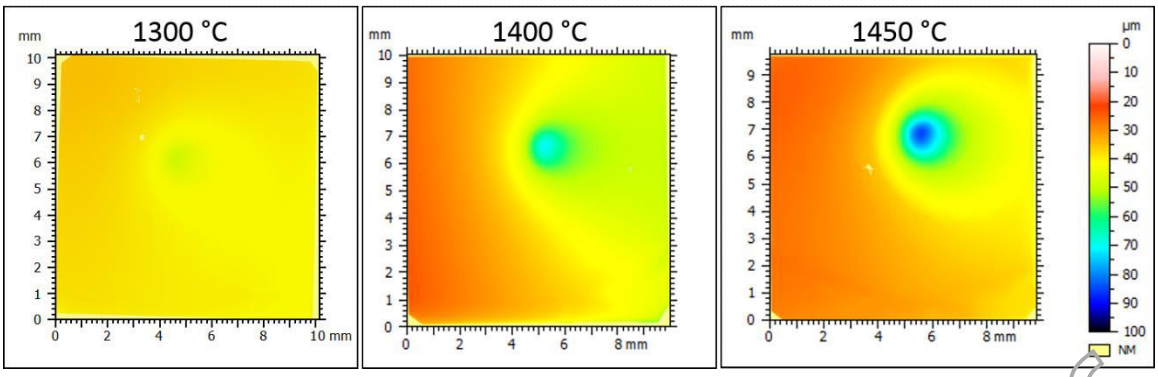

Figure 5. Profilometry maps for Al_2O_3 (0001) after steam exposure for 24h at 1300 °C, 1400 °C, and 1450 °C.

Figure 6 displays the profilometry map and recession linescan for Al_2O_3 (0001) exposed to steam at 1300 °C for 24 hours, where the recession depth color scale has been adapted to better display the recession behavior across the sample. A linescan was taken across the arrow on the profilometry map and is compared to the square root of the calculated ANSYS steam velocity, in accordance with the theoretical velocity dependence from Equation 2. Material recession is plotted to provide a direct comparison to calculated steam velocities. The impingement site displayed a maximum recession of 14.3 µm at a gas velocity of 184 m/s.

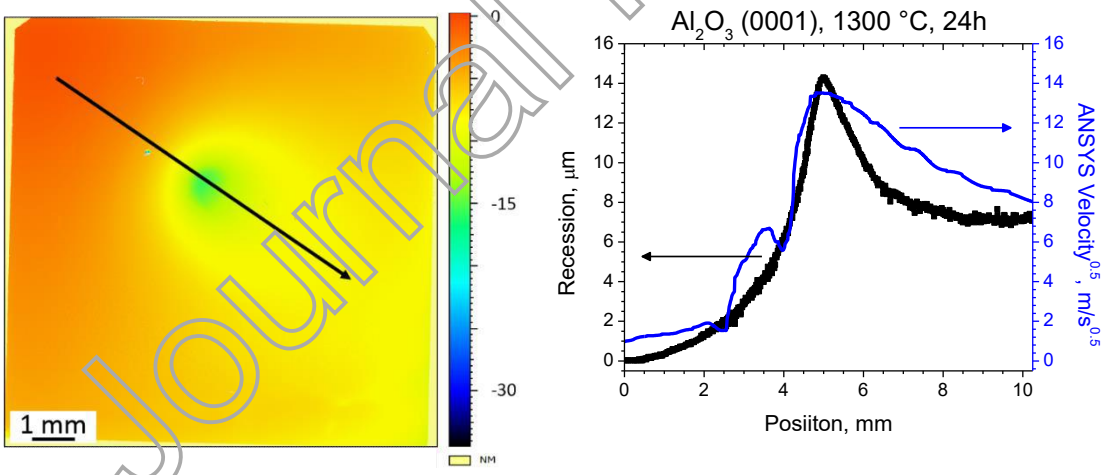

Figure 6. Surface topography of Al_2O_3 (0001) exposed to steam at 1300 °C for 24h. Recession depths along the arrow are plotted against position and compared to the square root of the calculated ANSYS steam velocity distribution through the impingement site.

Maximum recession and specific mass loss data for each sample are presented in Figure 7 and Figure 8, respectively. Mass loss data normalized to the total area of one side of the coupon

were considered accurate due to the minimal sample cracking and lack of additional sample reactions with furnace ware. Linear reaction rates for both mass loss and maximum recession data are presented in Table 2. The calculated velocities for each temperature are also presented, as maximum steam velocities varied between 173 – 204 m/s for the 1200 °C – 1450 °C temperature range.

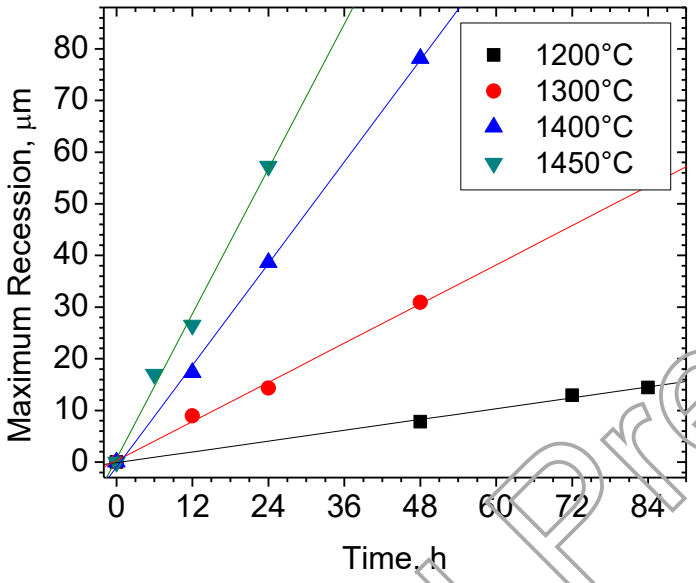

Figure 7. Maximum recession depth plotted against time (hours) for (0001) Al_2O_3 reactions with high-velocity steam.

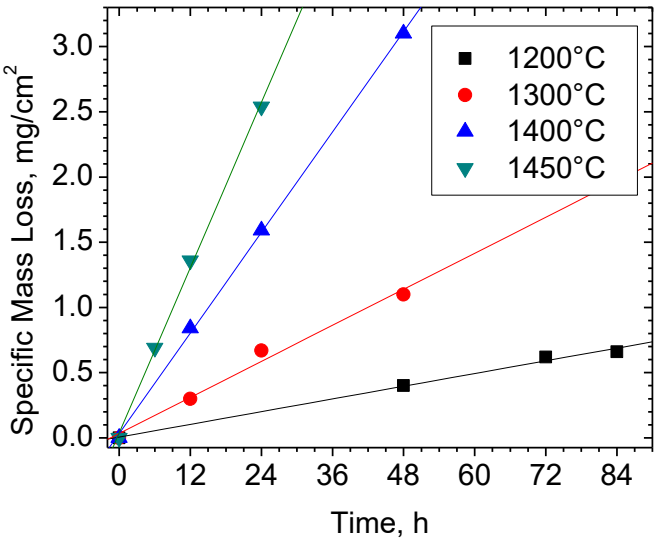

Figure 8. Specific mass loss plotted against time (hours) for (0001) Al_2O_3 reactions with high-velocity steam.

Table 2. Linear reaction rates for Al_2O_3 (0001) after high velocity steam exposures.

Temperature	Linear Reaction Rates		Maximum Velocity
°C	mg/cm^{2}h	μm/h	m/s
1200	8.1 ± 0.2 x10^{-3}	0.18 ± 0.01	173
1300	2.3 ± 0.2 x10^{-2}	0.63 ± 0.03	184
1400	6.4 ± 0.1 x10^{-2}	1.64 ± 0.04	196
1450	1.05 ± 0.03 x10^{-1}	2.3 ± 0.1	204

4. Analysis

For a saturated steam environment, the equilibrium constant, K_{eq}, for the chemical reaction in Equation 4 simplifies to the equilibrium partial pressure of the hydroxide species (P_{Eq}) being produced, $Al(OH)_3$ (g). Gibbs Free Energy, ΔG, is related to the equilibrium constant through Equation 5, where R is the universal gas constant and T is temperature in Kelvin.

$$\Delta G = -RTln(K_{Eq}) = -RTln(P_{Eq}) \quad (5)$$

The temperature dependences for the mass loss and maximum recession data were also dependent on gas phase interdiffusion through a boundary layer created by the steam flow, and

thus require an additional $T^{3/2}$ temperature dependence from D_{AB} through Chapman-Enskog Theory, as shown in Equation 6.

$$k_l \propto \left[D_{AB} \times \exp\left(-\frac{\Delta H_{rxn}}{RT}\right)\right] \propto T^{\frac{3}{2}} \exp\left(-\frac{\Delta H_{rxn}}{RT}\right) \quad (6)$$

FactSage equilibrium partial pressures from Figure 4 were used to calculate a theoretical temperature dependence for the chemical reaction in Equation 4 through the following relationship:

$$P_{Eq} \propto \exp\left(-\frac{\Delta H_{rxn}}{RT}\right) \quad (7)$$

where ΔH_{rxn} is the reaction enthalpy. A reaction enthalpy of 192 kJ/mol was calculated from Equation 7 for the FactSage SGPS thermodynamic data. FactSage data represent the equilibrium concentration of species in thermodynamic equilibrium and thus do not incorporate the $T^{3/2}$ temperature dependence from gas phase interdiffusion.

Temperature dependences and calculated reaction enthalpies for (0001) plane Al_2O_3 exposed to high-velocity steam and FactSage SGPS calculations are presented in Figure 9 with slope analysis in Table 3. Mass loss and maximum recession data displayed reaction enthalpies of 197 ± 5 kJ/mol and 200 ± 10 kJ/mol, respectively, in good agreement with each other. Both values were slightly higher than the reaction enthalpy of 192 kJ/mol determined from FactSage, which may have been due to the slightly increasing steam velocity with increasing furnace temperature.

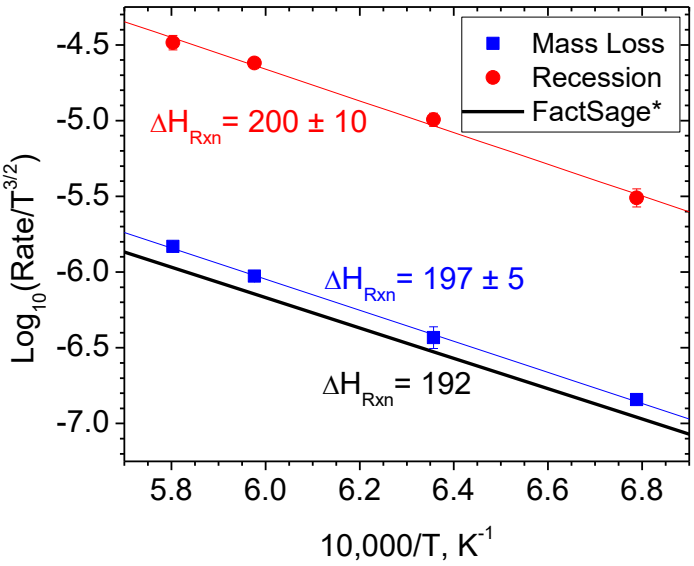

*Figure 9. Temperature dependences for specific mass loss and maximum recession data for Al_2O_3 in steam, compared to FactSage SGPS calculations. *FactSage SGPS data are presented as Log_{10}(rate) as the calculations only utilize the equilibrium concentration of species at the oxide-steam interface.*

Table 3. Slopes and reaction enthalpies for the temperature dependences plotted in Figure 9 for the reactions of Al_2O_3 with steam.

	Temperature Dependence		
	mg/cm²h	µm/h	FactSage
Slope	-1.03 ± 0.03	-1.05 ± 0.05	-1.00135
ΔH_{rxn}, kJ/mol	197 ± 5	200 ± 10	192

5. Discussion

5.1 Quantitative Accuracy of the Steamjet for Single Binary Metal Oxides

Rapid steamjet testing of (0001) Al_2O_3 in high-velocity steam was performed to calculate the reaction enthalpy from the temperature dependence of the reaction with steam. Experimental and calculated reaction enthalpies for $Al(OH)_3$ (g) formation are presented in Table 4. An average value was determined from the literature to be 203 ± 15 kJ/mol. Mass loss and recession data from this work resulted in reaction enthalpies of 197 ± 5 kJ/mol and 200 ± 10 kJ/mol,

respectively, which were both in agreement with the reaction enthalpies determined from FactSage and the literature.

Table 4. Reaction enthalpies for the steam reaction with Al_2O_3 to form $Al(OH)_3$ (g).

ΔH_{rxn}, kJ/mol	Notes
229	Ab Initio [19]
210 ± 20	Thermogravimetric analysis (0001) Al_2O_3 [20]
210 ± 9	Transpiration measurements of $CaAl_4O_7$ [21]
192	FactSage SGPS Database
191	Calculated [22]
185	Calculated [17]
Average	
203 ± 15	

The clear presence of a velocity dependence on the recession rate suggests a gas-phase diffusion mechanism is controlling the steam reaction with Al_2O_3. Linear reaction rates were measured from both specific mass loss and the maximum recession data, confirming that the reaction does not slow down with increasing exposure time. The temperature dependence determined through this work confirm that transport of $Al(OH)_3$ (g) though a steam boundary layer is the rate-limiting step for the Al_2O_3 volatilization reaction in steam.

5.2 Interpretation of Volatility from Complex Oxides

SOFC environments have near stagnant steam velocities such that thermogravimetric analysis remains an acceptable measurement technique for determining temperature dependences for oxide-steam reactions. Yet, an accelerated reaction can be accurately performed with high-velocity steam exposures to predict lifetimes of components intended for long-term use. High-velocity steam environments, such as turbine engine components, require a high-velocity testing apparatus such as the steamjet to better model the combustion environment. For complex silicate

environmental barrier coatings (EBCs), such as $HfSiO_4$ and $Yb_2Si_2O_7$, the predicted gas product phase was $Si(OH)_4$ (g) due to the selective removal of SiO_2 to produce porous HfO_2 and Yb_2SiO_5 reaction products on the sample surfaces [14], [15]. The stability of the reaction product layer implied negligible volatilization of HfO_2 and Yb_2O_3. Calculated reaction enthalpies for $HfSiO_4$ and $Yb_2Si_2O_7$ were 207 ± 39 kJ/mol and 207 ± 5 kJ/mol, respectively, while the calculated reaction enthalpy for SiO_2 is near 56 kJ/mol [23]. The temperature dependences for the $HfSiO_4$ and $Yb_2Si_2O_7$ reactions must then be linked to one of the following: 1. The transport of gas species through a porous reaction product layer grown on complex silicates after steam exposure, or 2. The volatilization reaction of SiO_2 from the complex silicates. By the kinetic theory of gases, gas transport has a temperature dependence of $T^{3/2}$ [13]. Based on the results of this study for c-plane sapphire recession, the temperature dependence and thus the reaction enthalpy of SiO_2 volatilization from complex silicates was measured correctly with the steamjet experimental setup. The reaction enthalpies for complex silicate compounds that produce a porous product layer with enhanced stability in steam environments must then result in significantly different values compared to that of pure SiO_2.

Other instances of the expected volatilization temperature difference for complex oxides can be found in the literature. The steam reaction for $CaAl_4O_7$ was utilized to accurately determine reaction enthalpies comparable to formation of $Al(OH)_3$ (g) through indirect transpiration measurements, as presented earlier [21]. Testing of complex oxides such as $CaAl_4O_7$ implies that compounds should display similar reaction enthalpies as their constituent volatile oxide species, consistent with experimentally observed volatilization and analysis of BSAS in high-velocity steam [16]. $CaAl_4O_7$ and BSAS both displayed volatilization of all constituent oxides, such that a porous reaction product was not present on the surface after steam

exposures and showed temperature dependent results in agreement with reaction enthalpies for steam reactions with all constituent oxides. Contrarily, Table 5 presents estimated reaction enthalpies for P_2O_5, Al_2O_3, and $AlPO_4$ (0.5 Al_2O_5·0.5 P_2O_5) provided by Meschter et al. [17]. The reaction enthalpies for P_2O_5 and Al_2O_3 are similar, despite their unique gas product species upon steam reaction and widely different melting temperatures. The calculated reaction enthalpy for $Al(OH)_3$ (g) in Table 5 is slightly lower than the average value shown previously in Table 4.

Table 5. Reaction enthalpies, steam reactions, and melting temperatures for P_2O_5, Al_2O_3, and $AlPO_4$, from [17].

Oxide	Reaction Enthalpy, kJ/mole	Reaction	Oxide Melting Temperature, °C
P_2O_5	173	0.5 P_2O_5 + 0.5 H_2O (g) = $PO_2(OH)$ (g)	340
Al_2O_3	185	0.5 Al_2O_3 + 1.5 H_2O (g) = $Al(OH)_3$ (g)	2072
$AlPO_4$	303	$AlPO_4$(c) + 0.5 H_2O (g) = 0.5 Al_2O_3 + $PO_2(OH)$ (g)	1800

Selective volatilization of P_2O_5 from $AlPO_4$ has been determined experimentally [24], where a porous Al_2O_3 product layer is present after steam exposures. Yet, the estimated reaction enthalpy for $AlPO_4$ does not agree with that of pure P_2O_5 and is not represented by any form of rule of mixtures between P_2O_5 and Al_2O_3. While the reaction enthalpies presented are not experimentally determined, the volatilization behavior of $AlPO_4$ is consistent with the current hypothesis that complex compounds that react with steam to form a porous product layer may not display similar reaction enthalpies as their individual volatile components.

6. Conclusion

Rapid high-velocity steam testing was performed for (0001) Al_2O_3 from 1200 °C – 1450 °C. Linear recession kinetics were attributed to the formation of $Al(OH)_3$ (g). The temperature dependences for specific mass loss and maximum recession data resulted in enthalpies of 197 ± 5

kJ/mol and 200 ± 10 kJ/mol, respectively. Reaction enthalpies in this work were in agreement with thermodynamic calculations and literature values, which support the quantitative nature of the steamjet experimental setup and verifies transport of $Al(OH)_3$ (g) through a gas boundary layer as the rate-limiting step for Al_2O_3 exposed to high-velocity water vapor. The results of this work suggest that complex silicate compounds, such as $HfSiO_4$ and $Yb_2Si_2O_7$, show temperature dependences related to production of $Si(OH)_x$ (g) species, however the predicted temperature dependence for $Si(OH)_x$ (g) transport has not been observed experimentally. The origin of differing enthalpies for complex oxide-steam interactions when a porous reaction product with steam resistance is produced on the sample surface is not yet understood.

Declaration of interests

The authors declare that they have no known competing financial interests or personal relationships that could have appeared to influence the work reported in this paper.

7. Acknowledgements

This work was funded through the Office of Naval Research Award #N000141712280 with program manager Dr. David Shifler and the National Science Foundation DMREF: Collaborative Research: GOALI: Accelerating Discovery of High Entropy Silicates for Extreme Environments, Award #1921973. The authors would like to acknowledge the Nanoscale Materials Characterization Facility at the University of Virginia for supporting this research through characterization equipment.

8. References

[1] H. Yokokawa *et al.*, "Thermodynamic considerations on Cr poisoning in SOFC cathodes," *Solid State Ionics*, vol. 177, no. 35, pp. 3193–3198, Nov. 2006, doi: 10.1016/j.ssi.2006.07.055.

[2] D. J. Young and B. A. Pint, "Chromium Volatilization Rates from Cr2O3 Scales into Flowing Gases Containing Water Vapor," *Oxid Met*, vol. 66, no. 3–4, pp. 137–153, Nov. 2006, doi: 10.1007/s11085-006-9030-1.

[3] T. Zhang, W. G. Fahrenholtz, S. T. Reis, and R. K. Brow, "Borate Volatility from SOFC Sealing Glasses," *Journal of the American Ceramic Society*, vol. 91, no. 8, pp. 2564–2569, 2008, doi: 10.1111/j.1551-2916.2008.02479.x.

[4] X. Yin, L. Bencze, V. Motalov, R. Spatschek, and L. Singheiser, "Thermodynamic perspective of Sr-related degradation issues in SOFCs," *International Journal of Applied Ceramic Technology*, vol. 15, no. 2, pp. 380–390, 2018, doi: 10.1111/ijac.12809.

[5] N. Al Nasiri, N. Patra, D. D. Jayaseelan, and W. E. Lee, "Water vapour corrosion of rare earth monosilicates for environmental barrier coating application," *Ceramics International*, vol. 43, no. 10, pp. 7393–7400, Jul. 2017, doi: 10.1016/j.ceramint.2017.02.123.

[6] S. Ueno, D. D. Jayaseelan, H. Kita, T. Ohji, and H. T. Lin, "Comparison of Water Vapor Corrosion Behaviors of $Ln_2Si_2O_7$ (Ln=Yb and Lu) and $ASiO_4$ (A=Ti, Zr and Hf) EBC's," *Key Engineering Materials*, vol. 317–318, pp. 557–560, 2006, doi: 10.4028/www.scientific.net/KEM.317-318.557.

[7] N. Maier, K. G. Nickel, and G. Rixecker, "High temperature water vapour corrosion of rare earth disilicates $(Y,Yb,Lu)_2Si_2O_7$ in the presence of $Al(OH)_3$ impurities," *Journal of the European Ceramic Society*, vol. 27, no. 7, pp. 2705–2713, Jan. 2007, doi: 10.1016/j.jeurceramsoc.2006.09.013.

[8] E. J. Opila and R. E. Hann, "Paralinear Oxidation of CVD SiC in Water Vapor," *Journal of the American Ceramic Society*, vol. 80, no. 1, pp. 197–205, 1997, doi: 10.1111/j.1151-2916.1997.tb02810.x.

[9] M. K. Ferber and H. T. Lin, "Environmental Characterization of Monolithic Ceramics for Gas Turbine Applications," *Key Eng. Mat.*, vol. 287, pp. 367–380, Jun. 2005, doi: 10.4028/www.scientific.net/KEM.287.367.

[10] R. A. Golden and E. J. Opila, "A method for assessing the volatility of oxides in high-temperature high-velocity water vapor," *Journal of the European Ceramic Society*, vol. 36, no. 5, pp. 1135–1147, Apr. 2016, doi: 10.1016/j.jeurceramsoc.2015.11.016.

[11] C. G. Parker and E. J. Opila, "Stability of the Y_2O_3-SiO_2 system in high-temperature, high-velocity water vapor," *J Am Ceram Soc*, p. jace.16915, Dec. 2019, doi: 10.1111/jace.16915.

[12] E. J. Opila, "Variation of the Oxidation Rate of Silicon Carbide with Water-Vapor Pressure," *Journal of the American Ceramic Society*, vol. 82, no. 3, pp. 625–636, 1999, doi: 10.1111/j.1151-2916.1999.tb01810.x.

[13] J. Welty, "Fundamentals of Momentum, Heat and Mass Transfer, 5th Edition," p. 729.

[14] M. J. Ridley and E. J. Opila, "Thermomechanical and Thermochemical Stability of $HfSiO_4$ for Environmental Barrier Coating Applications," *J Am Ceram Soc*, 2020, doi: 10.1111/jace.17729.

[15] M. Ridley and E. Opila, "Thermochemical stability and microstructural evolution of $Yb_2Si_2O_7$ in high-velocity high-temperature water vapor," *Journal of the European*

Ceramic Society, vol. 41, no. 5, pp. 3141–3149, May 2020, doi: 10.1016/j.jeurceramsoc.2020.05.071.
[16] M. J. Ridley and E. J. Opila, "High-Temperature Water-Vapor Reaction Mechanism of Barium Strontium Aluminosilicate (BSAS)," *Manuscript in Progress*.
[17] P. J. Meschter, E. J. Opila, and N. S. Jacobson, "Water Vapor–Mediated Volatilization of High-Temperature Materials," *Annu. Rev. Mater. Res.*, vol. 43, no. 1, pp. 559–588, Jul. 2013, doi: 10.1146/annurev-matsci-071312-121636.
[18] S. L. dos Santos e Lucato, O. H. Sudre, and D. B. Marshall, "A Method for Assessing Reactions of Water Vapor with Materials in High-Speed, High-Temperature Flow," *J. Am. Ceram. Soc.*, vol. 94, pp. s186–s195, Jun. 2011, doi: 10.1111/j.1551-2916.2011.04556.x.
[19] M. D. Allendorf, C. F. Melius, B. Cosic, and A. Fontijn, "BAC-G2 Predictions of Thermochemistry for Gas-Phase Aluminum Compounds," *J. Phys. Chem. A*, vol. 106, no. 11, pp. 2629–2640, Mar. 2002, doi: 10.1021/jp013128r.
[20] E. J. Opila and D. L. Myers, "Alumina Volatility in Water Vapor at Elevated Temperatures," *Journal of the American Ceramic Society*, vol. 87, no. 9, pp. 1701–1705, 2004, doi: https://doi.org/10.1111/j.1551-2916.2004.01701.x.
[21] A. Hashimoto, "The effect of H_2O gas on volatilities of planet-forming major elements: I. Experimental determination of thermodynamic properties of Ca-, Al-, and Si-hydroxide gas molecules and its application to the solar nebula," *Geochimica et Cosmochimica Acta*, vol. 56, no. 1, pp. 511–532, Jan. 1992, doi: 10.1016/0016-7037(92)90148-C.
[22] L. V. Gurvich, I. V. Veyts, and C. B. Alcock, "Thermodynamic Properties of Individual Substances," *Begell House*, vol. Vol. 3, no. Part 1, pp. 138, 150–151, 1996.
[23] A. V. Plyasunov, "Thermodynamic properties of H_4SiO_4 in the ideal gas state as evaluated from experimental data," *Geochimica et Cosmochimica Acta*, vol. 75, no. 13, pp. 3853–3865, Jul. 2011, doi: 10.1016/j.gca.2011.04.016.
[24] X.-H. Chen, L.-F. Cheng, Y.-G. Wang, L.-T. Zhang, Z.-L. Hong, and Y.-H. Wu, "Corrosion Behavior of $AlPO_4$ as Environmental Barrier Coating in Water Vapor Environment," *Journal of Inorganic Materials*, vol. 24, no. 2, pp. 397–401, 2009.